



# Optimized AC-Circulating Current for Active Cross-Connected Modular Multilevel Converter in Medium-Voltage Motor Drive Applications

Tan Luong Van<sup>1,\*</sup>

## ARTICLE INFO

### Article history:

Received: 23 February 2024

Revised: 12 April 2024

Accepted: 26 May 2024

Online: 20 June 2024

### Keywords:

Current reduction

Low-speed operation

Modular multilevel converters

## ABSTRACT

This paper proposes an advanced scheme designed to optimize the ac-circulating current for the active cross-connected modular multilevel converters (AC-MMCs). Rather than entirely mitigating the submodule capacitor voltage ripples, this approach controls them to fluctuate within a predefined limit. To achieve that, the ac-circulating current, redistributing the power imbalance between upper and lower arms, is analyzed and designed appropriately. Then, the current stresses on the switching devices and inductors are reduced, resulting in the improvement of power losses. Simulation results and discussion based 4160-V/1-MW simulation model of active cross-connected MMC have been provided to validate the feasibility of the proposed control scheme.

## 1. INTRODUCTION

Through the past decade, modular multilevel converters (MMCs) have been leading commercial success in medium to high voltage applications due to their advantages such as low-distorted output voltages and modularity. Therefore, they are researched and conducted in the fields of high-voltage direct-current transmission systems [1–4] and static synchronous compensators [5], [6]. Its application in medium-voltage adjustable-speed motor drives is also a promising field [7–22]. Nevertheless, it is different from implementing MMCs in HVDCs and STATCOMs that the fundamental frequency or speed of motor drive should be varied from zero to rated value, which leads to large submodule capacitor voltage ripple (SMCVR) at low-speed range [7–14].

In [8], [9], [13], [14], improved control methods, which can suppress the magnitude of capacitor voltage ripples, have been introduced. In [8], [9], the common-mode voltage (CMV) and ac-circulating current are introduced into MMCs, helping to mitigate SMCVRs. However, the extra CMV leads to the deterioration of motor bearing and winding insulation. In [13], [14], SM capacitor voltage (SMCV) is allowed to fluctuate within a predefined limit. Thus, the arm current or the CMV can be reduced. Nevertheless, the CMV on the AC side is not significantly improved.

Meanwhile, MMC topologies with the additional components have been studied to reduce SMCVRs without

injection of the CMV [15–18]. However, SMCVRs are still large at a low-speed range. Flying-capacitors MMC were suggested in [19], [20], where they are used to link both arms in each phase, resulting in balance power difference within each phase on account of the high-frequency current. However, the amplitude of injected high-frequency ac-circulating current is dominant. To reduce this amplitude, a square-wave method has been introduced [21], which required a complicated controller design. An active cross-connected MMC (AC-MMC) [22], where a series of SMs is implemented to link the center taps, has been proposed to obtain a lower ac-circulating level. However, further lowering the level of ac-circulating current can enhance the efficiency of the system.

This paper aims to reduce the amplitude of the ac-circulating current by permitting the SMCV to fluctuate within a defined limit instead of completely eliminating it. Consequently, the peak current experienced by the semiconductor devices and inductors can be further decreased. This demonstrates that the proposed control strategy results in a 39% enhancement in reducing current stresses on the semiconductor devices and inductors compared to the traditional method. Consequently, there is a substantial improvement in inductor volume and power losses. Simulation has been performed to confirm the validation of the proposed scheme. Furthermore, a comparison of power losses with the conventional method is also presented to validate the system efficiency of incorporating the proposed scheme.

<sup>1</sup>Department of Electrical and Electronic Engineering, Ho Chi Minh city University of Industry and Trade, Ho Chi Minh city, 760310, Vietnam.

\*Corresponding author: Tan Luong Van; Phone: +84-909-653-157; Email: luongvt@huit.edu.vn.

This paper is organized as follows. The mitigation of SMCVR in AC-MMC under low-speed operation is described in Section 2. Next, the optimized AC-circulating current control for AC-MMC is analyzed in Section 3. In Section 4, the simulation results and discussion for the AC-MMC system with 36 SMs are provided. Finally, the conclusion is presented in the last Section.

## 2. MITIGATION OF SMCVR IN AC-MMC UNDER LOW-SPEED OPERATION

### 2.1. Circuit configuration

The AC-MMC topology is shown in Fig. 1 [22], where each leg consists of submodules (SM) and four inductors. The SMs used in this paper are half-bridge SMs, which save cost as well as volume of system. Those SM are configured into half-arms and a branch of series connected half-bridge SM. To alleviate the SMCVRs, the imbalanced power between upper and lower arms are redistributed through this branch. In Fig. 1,  $N$  is a total number of SMs in each leg without including SMs in branch, and  $0.5N$  SMs are implemented in the branch. Induction motor inputs ( $x$ :  $a$ ,  $b$ ,  $c$ ) are from the output of each leg.

### 2.2. Mitigation of SMCVR under low-speed operation

In Fig. 1,  $i_{UP1,x}$ ,  $i_{UP2,x}$ ,  $i_{LO1,x}$ ,  $i_{LO2,x}$  and  $v_{UP1,x}$ ,  $v_{UP2,x}$ ,  $v_{LO1,x}$ ,  $v_{LO2,x}$  are the current and voltage of four half-arms in each leg, respectively. In addition, are the currents conducting in those half-arms. Those variables are given as:

$$i_{UP1,x} = i_{xdc} + 0.5i_x + i_{inj,x} \quad (1)$$

$$i_{UP2,x} = i_{xdc} + 0.5i_x - i_{inj,x} \quad (2)$$

$$i_{LO1,x} = i_{xdc} - 0.5i_x - i_{inj,x} \quad (3)$$

$$i_{LO2,x} = i_{xdc} - 0.5i_x + i_{inj,x} \quad (4)$$

$$v_{UP1,x} = 0.25V_{dc} - 0.5v_x - v_{inj} \quad (5)$$

$$v_{UP2,x} = 0.25V_{dc} - 0.5v_x + v_{inj} \quad (6)$$

$$v_{LO1,x} = 0.25V_{dc} + 0.5v_x - v_{inj} \quad (7)$$

$$v_{LO2,x} = 0.25V_{dc} + 0.5v_x + v_{inj} \quad (8)$$

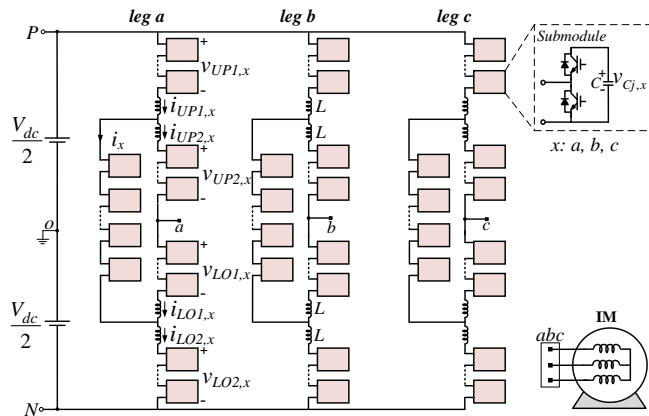


Fig. 1. Circuit structure of AC-MMC.

where,  $V_{dc}$  represents the dc-link input voltage of the AC-MMC along with the dc input current per leg,  $i_{xdc}$ . As illustrated in Fig. 1,  $v_x$  and  $i_x$  denote the phase voltage and current of converter,  $v_{inj,x}$  signifies the injected high-frequency voltage, and  $i_{inj,x}$  refers to the ac-circulating current.  $v_x$ ,  $i_x$ ,  $i_{inj,x}$  and  $v_{inj,x}$  are:

$$v_x = V_{ph} \sin(\omega t + \theta) \quad (9)$$

$$i_x = I_{ph} \sin(\omega t + \theta - \varphi) \quad (10)$$

$$i_{inj,x} = I_{inj,x} \sin(\omega_h t) \quad (11)$$

$$v_{inj,x} = V_{inj,x} \sin(\omega_{inj,x} t) = 0.25(1-m)V_{dc} \sin(\omega_{inj,x} t) \quad (12)$$

where,  $V_{ph}$  and  $I_{ph}$  represent the magnitudes of phase voltage and current of converter,  $V_{inj,x}$  and  $I_{inj,x}$  denote the magnitudes of voltage and current, and  $\omega_{inj,x}$  is the injected frequency, which is at least two times of rated fundamental frequency.

From (1) and (5), the SMCVR is derived from the instantaneous power fluctuation,  $\tilde{p}_{UP1,x}$ , and the energy fluctuation,  $\tilde{E}_{UP1,x}$ . It is identical for other half-arms because of the symmetry of circuit. The instantaneous power fluctuation is derived:

$$\tilde{p}_{UP1,x} = 0.125V_{dc}i_x - 0.5v_x i_{xdc} - v_{inj,x}i_x + 0.25V_{dc}i_{xdc} - 0.25v_x i_x \quad (13)$$

In (13), the second term is negligible due to its small value, and the fourth term is equal to the last term because of the equilibrium of power between the input and output sides. (13) is derived as:

$$\tilde{p}_{UP1,x} = 0.125V_{dc}i_x - 0.5V_{inj,x}I_{inj,x} - 0.5V_{inj,x}I_{inj,x} \sin(2\omega_{inj}t) \quad (14)$$

The first term, referred to as low-frequency power fluctuation (LFPF), can be entirely nullified by the addition of the second term through injected components. Following this, a third term remains, characterized by high-frequency fluctuations, leading to rapid charging and discharging (at a rate of  $\omega_h = 2\pi f_h$ ) of the SM capacitor. Consequently, SMCVRs have transitioned to a low.

## 3. OPTIMIZED AC-CIRCULATING CURRENT CONTROL FOR AC-MMC

### 3.1. Optimized AC-circulating current

Instead of alleviating the SMCVR completely, it can be mitigated partially. In (14), the adjustment ensures that  $0.5V_{inj,x}I_{inj,x}$  is proportionate to  $0.125V_{dc}i_x$  as:

$$0.5V_{inj,x}I_{inj,x} = \alpha 0.125V_{dc}i_x \quad (15)$$

where,  $\alpha$ , a coefficient varying from zero to one, defines the degree to which the LFPF is alleviated. When  $\alpha = 1$ , the injected components completely attenuate the LFPF. If  $\alpha = 0$ , the converter operates without any mitigation of SMCVR

from the injection. From (11), (12) and (15), the ac-circulating current reference is established as:

$$i_{inj,x}^* = \alpha I_{inj,x} \sin(\omega_{inj} t) = \alpha \frac{i_x}{1-m} \sin(\omega_{inj} t). \quad (16)$$

Substituting (10) and (15) into (14), the power fluctuation is rewritten as:

$$\tilde{p}_{UP1,x} = 0.125(1-\alpha)V_{dc}I_{ph} \sin(\omega t + \theta - \varphi). \quad (17)$$

The maximum value of energy fluctuation is derived as:

$$\tilde{e}_{UP1,x\_pp} = \frac{0.25(1-\alpha)}{\omega} V_{dc} I_{ph}. \quad (18)$$

Besides, the peak-to-peak energy fluctuation  $\tilde{e}_{xU1\_pp}$  also has a relationship with SMCVR as:

$$\begin{aligned} \tilde{e}_{UP1,x\_pp} &= \frac{N}{2} \left( \frac{1}{2} C(v_c + \Delta v_{sm})^2 - \frac{1}{2} C(v_c - \Delta v_{sm})^2 \right) \\ &= NCv_c \Delta v_{sm} \\ &= 0.5NCv_c \Delta v_{sm\_pp} \end{aligned} \quad (19)$$

Combining (18) and (19), the peak-to-peak SMCVR denoted as  $\Delta v_{sm\_pp}$ , as follows:

$$\Delta v_{sm\_pp} = \frac{0.5(1-\alpha)I_o}{\omega C}. \quad (20)$$

where,  $\alpha$  is derived as:

$$\alpha = 1 - \frac{2\omega C}{I_o} \Delta v_{sm\_pp}. \quad (21)$$

The determination of the  $\alpha$  value is influenced by the predetermined  $\Delta v_{sm\_pp}$  for the SMCVR, which should be lower than 20% of the nominal voltage of electrolytic capacitor of SM. At the low-speed operation, by predefining  $\Delta v_{sm\_pp}$ , the ac-circulating current reference in (16) is created for the controller and the SMCVR fluctuates within that range instead of complete alleviation. Therefore, the required ac-circulating current to keep converter operating at low-speed ranges can be reduced by the proposed control scheme.

### 3.2. Control Algorithm

In the presented block diagrams shown in Fig. 2, the leg-balancing control illustrated in Fig. 2(a) features the SMCV reference denoted by  $v_c^*$ , while the per phase average SMCV, represented by  $v_{c,x}^{avg}$ , is provided as:

$$v_{c,x}^{avg} = \frac{1}{2N} \sum_{j=1}^{2N} v_{cj,x}. \quad (22)$$

where,  $\Delta v_{ph,x}^*$  is a phase voltage command, which supports to regulate  $v_{c,x}^{avg}$  to follow  $v_c^*$ .

The optimized ac-circulating current control is depicted in Fig. 2(b), which is formed from (11) and (21),  $I_{xh} = i_x/(1-$

$m)$  is the magnitude of the injected current. The magnitude of the optimized ac-circulating current is regulated by  $\alpha$  before comparing with the  $i_{xh}$  feedback signal to generate an error for the controller. The controller provides a voltage command,  $\Delta v_{xh}^*$ , having high-frequency components to maintain SMCVR low.

Fig. 2(c) shows the half-arm balancing control, where the per half-arm average SMCV is:

$$v_{xgk}^{avg} = \frac{1}{0.5N} \sum_{j=1}^{0.5N} v_{cj,x}. \quad (23)$$

The average voltages of the two half-arms are compared to generate an error signal for the PI controller. Depending on the directions of the arm currents, compensating voltage commands  $\Delta v_{xU}^*$  and  $\Delta v_{xL}^*$  are either added or subtracted from the voltage reference to maintain the average voltages of the two half-arms at a low level.

An individual SM balancing control is shown in Fig. 2(d), where each SMCV,  $v_{cj,xg}$ , is adjusted to track the voltage reference  $v_c^*$ . Finally, all voltage commands are synthesized and normalized before transferring to the PWM generator.

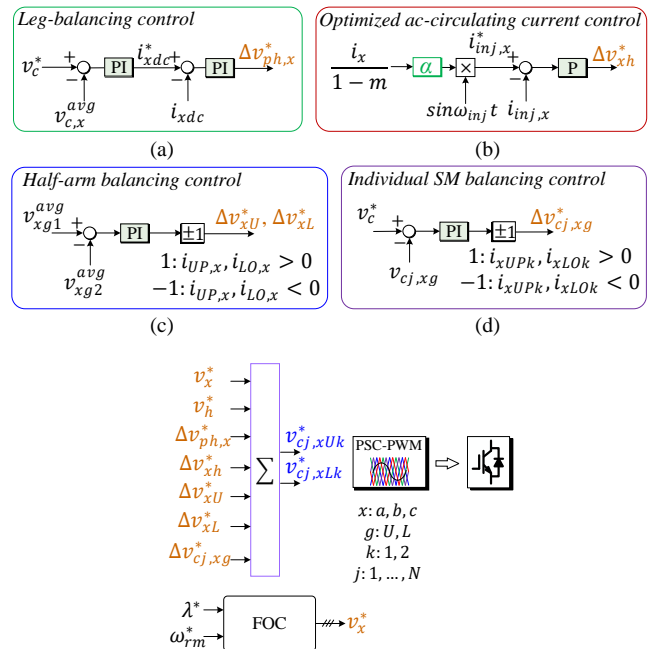


Fig. 2. Block diagram of the proposed control strategy.

### 4. SIMULATION RESULTS AND DISCUSSION

To confirm the feasibility of the proposed scheme, a simulation was conducted on the 4160-V/1-MW AC-MMC system with 36 SMs. An indirect vector control is implemented for the speed regulation of the motor. The system specifications are listed in Table 1 and 2.

Fig. 3 and Fig. 4 show performances of the AC-MMC with the conventional and proposed methods, respectively,

under  $T_L = 7490 \text{ N.m}$  and  $\omega_{rm} = 150 \text{ rpm}$ . The peak value of three-phase output current at full-load condition is 212 A shown in Fig. 3(a) and Fig. 4(a). In the conventional method, the LFPF is eliminated by the injection of the high-frequency terms, that leads to the low SMCVR with a value of 110 V of  $\Delta v_{sm\_pp}$  as illustrated in Fig. 3(d). On the contrary, the LFPF generating at the low-speed region is partially mitigated with  $\alpha = 0.62$  in the proposed scheme. Thus, the SMCVR fluctuates with a peak-to-peak value of 305 V which is close to the defined range,  $\Delta V_{c\_pp\_de}$ , of 300 V in Fig. 4(d). Fig. 4(b) demonstrates performance of ac-circulating current control in phase- $a$ ,  $i_{inj,a}$ , where the peak value is 160 A. It is like other phases. Fig. 3(b) illustrates the maximum value of  $i_{inj,a}$  in the conventional method is 325 A. The reduction of  $i_{ah}$  helps to decrease the current conducting through half-arms, leading to mitigate current amplitudes on semiconductor devices and inductors. In Fig. 3(c) and Fig. 4(c), the peak value of half-arm currents,  $i_{xUP1/2}$ , of the proposed control is 280 A, which is reduced by 39% compared to those values in the conventional method (460 A).

**Table 1. Converter specifications**

Parameters	Symbols	Values
DC-link voltage	$V_{dc}$	7000 V
Half-arm inductance	$L$	2.5 mH
Number of SMs per arm	$N$	4
SM capacitance	$C$	2700 $\mu\text{F}$
SM capacitor voltage reference	$v_c^*$	1750 V
Defined limit of peak-to-peak voltage ripple of capacitor	$\Delta V_{c\_pp\_de}$	300 V
Carrier frequency	$f_c$	2000 Hz
Injected frequency	$f_{inj}$	1 Hz

**Table 2. Motor specifications**

Parameters	Symbols	Values
Output power	$P_o$	1250 hp
Rated voltage	$V_{LL}$	4160 V
Rated current	$I_{rated}$	150 A
Rated frequency	$f_o$	60 Hz
Rated speed	$\omega_{m,rated}$	1189 rpm
Rated torque	$T_{rated}$	7490 N.m

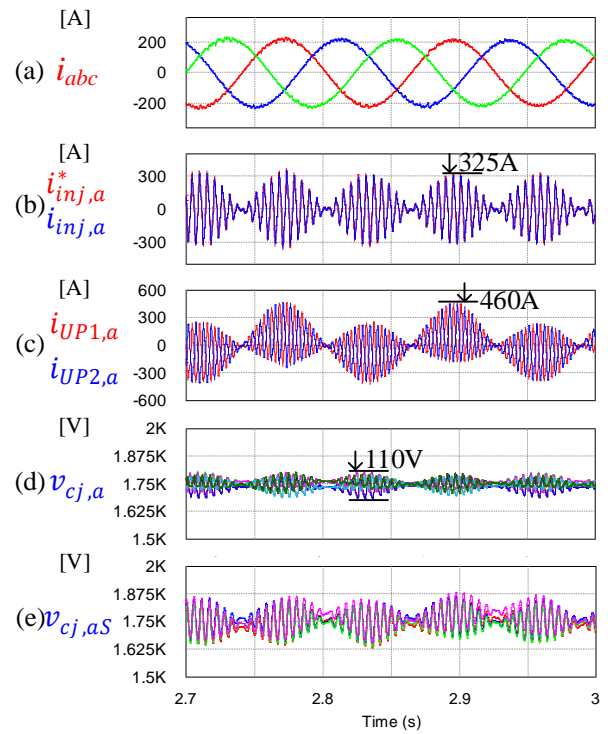


**Fig. 3. The conventional method.**

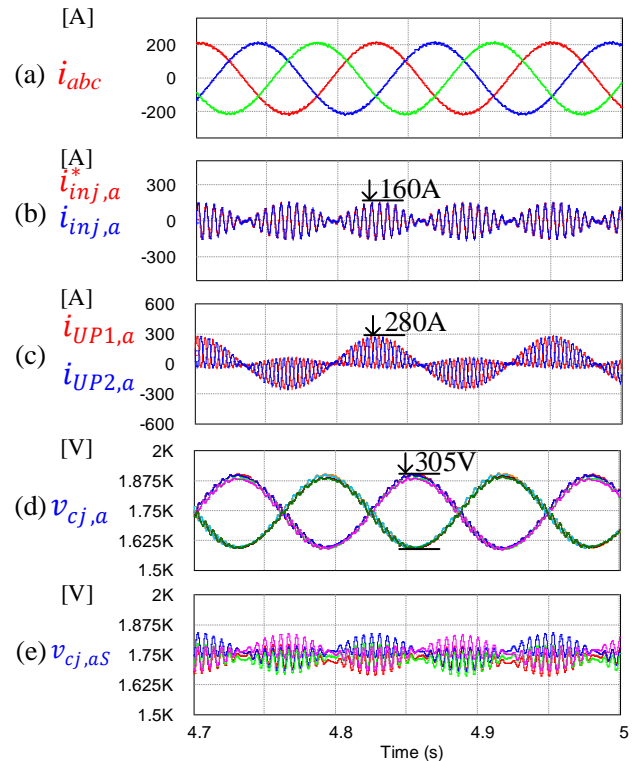


**Fig. 4. The proposed control strategy.**

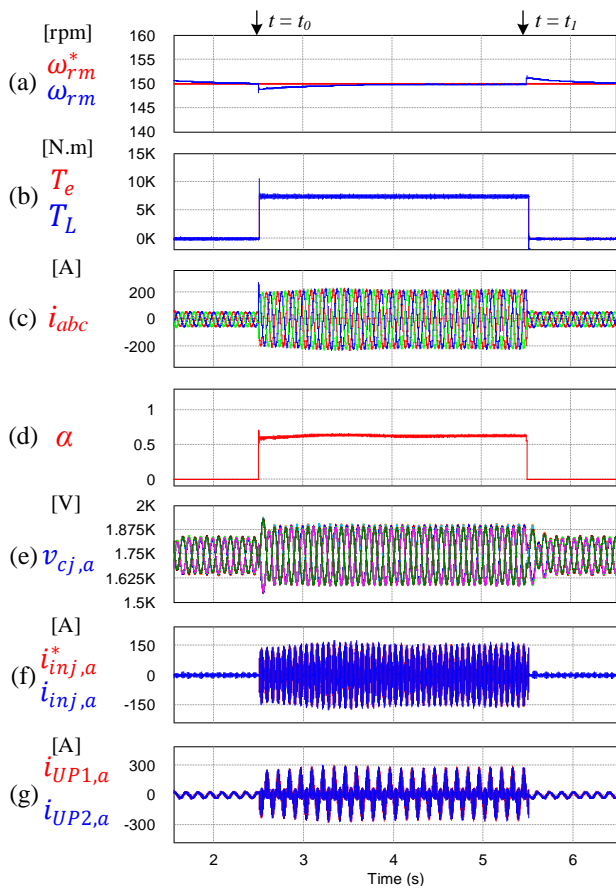


**Fig. 5. The proposed control strategy at  $\omega_{rm} = 150$  rpm with load change.**

Fig. 5 shows result of the proposed strategy at  $\omega_{rm} = 150$  rpm (0.1 p.u.) when a load torque undergoes an abrupt change from  $T_L = 0$  N.m to  $T_L = 7490$  N.m at  $t = t_0$  and then to  $T_L = 0$  N.m at  $t = t_1$ . Fig. 5(a) demonstrates that the motor speed closely tracks its reference, where values of undershoot or overshoot at the transient is around 1.5 rpm. Fig. 5(b) shows motor and load torque with 7490 N.m of full-load condition. Fig. 5(c) and (d) illustrate  $i_{abc}$  and coefficient  $\alpha$ . It can be seen that  $\alpha$  is equal to zero at no load condition since the output current level at that period is not high enough to cause the SMCVs to be fluctuated. Thus, the SMCVs are regulated well at  $v_c^* = 1750$  V with voltage ripple of 185 V. When  $T_L = 7490$  N.m, the coefficient  $\alpha$  is abruptly updated to a new value of 0.62 to keep the SMCVR within the defined range (300 V). Fig. 5(f) and (g) shows  $i_{inj,a}$  and  $i_{aUPk}$  in the upper arm of leg- $a$ . Due to no injection of the high-frequency component ( $\alpha = 0$ ), the ac-circulating current is almost zero. It helps to improve loss significantly compared with the conventional method which always injects high-frequency current and voltage to alleviate SMCVR. In addition, the converter and motor perform well without any injection.

Fig. 6 illustrates the simulation result of the acceleration process under  $T_L = 0$  N.m. In Fig. 6(a),  $\omega_{rm}$  increases from

zero at  $t = t_0$  to the nominal speed of 1189 rpm at  $t = t_2$ . The output currents are illustrated in Fig. 6(b), the inrush current should be high enough for the start-up of the motor (300 A of peak value). In Fig. 6(c),  $v_a$  voltage is illustrated, where the number of voltage level increases as motor speed rises. Finally, the obtained voltage level is five since the PSC-PWM has been implemented with same angle for both arms in each leg. Fig. 6(d) shows the coefficient  $\alpha$ , where  $\alpha = 1$  at very low speed. The coefficient  $\alpha$  reaches to zero when  $\omega_{rm} = 291$  rpm at  $t = t_1$ , since the motor speed is enough high according to (20). In addition, the SMCVR decreases as the motor speed increase; thus, the SMCVR becomes lower naturally as the speed increases further without any injection of high-frequency component as illustrated in Fig. 6(g). Fig. 6(e) and (f) shows the  $i_{inj,a}$  and  $i_{aUPk}$  in phase- $a$ . At  $\alpha = 0$ , there is no ac-circulating current within a leg, which also helps to reduce the current amplitude conducting through switching devices and inductors, leading to improve system efficiency.

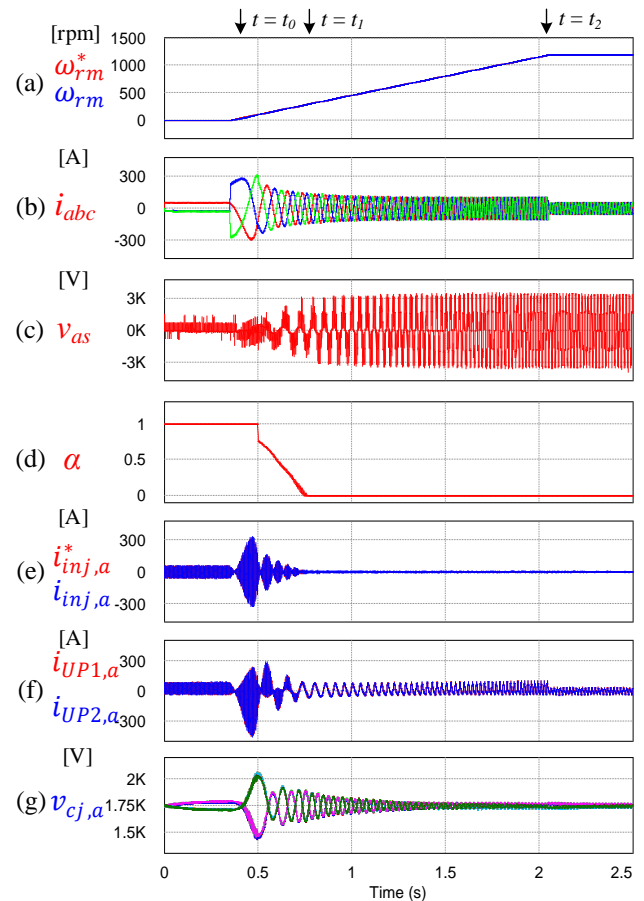


**Fig. 6. The accelerating process.**

To assess the effectiveness of the system, the power dissipation of both traditional and suggested approaches was examined. This analysis involved the utilization of the Infineon IGBT FF450R33T3E3 (rated at 3300 V/450 A) in the AC-MMC system [23]. The thermal module of PSIM was employed to compute both conduction and switching

losses [24]. The conduction loss of the IGBT component was determined based on the device's saturation voltage and the collector current [23]. The IGBT's switching loss was computed by considering the turn-on and turn-off losses. Fig. 7 illustrates a comparison of power losses between both methods at full-load conditions. The graph suggests that proposed approach suggests a higher efficiency than that of the traditional method. At the high-speed range, power losses of both methods are identical as the injection method has not been implemented, and the voltage across SM capacitors naturally balances with low ripples.

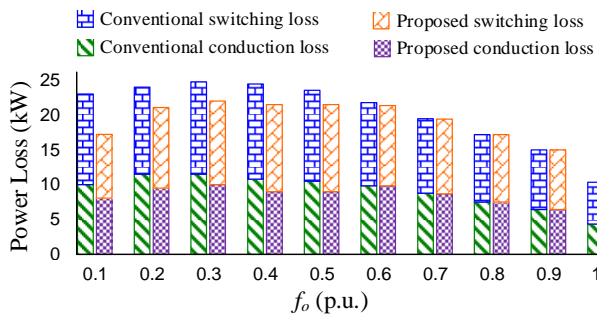


Fig. 7. Switching and conduction losses comparison between the proposed and conventional methods.

## 5. CONCLUSIONS

In this paper, the optimized ac-circulating current is proposed for the control strategy of AC-MMC. Instead of canceling SMCV ripples completely, they are controlled to fluctuate within the predefined range, resulting in the reduction of the power redistribution within each leg. It has been performed in the simulation results, where the current amplitudes on the semiconductor devices and inductors are reduced by around 39% compared with the existing method. Therefore, the system loss can be improved significantly. In addition, the proposed approach also was confirmed by simulation results with conditions of load change and acceleration.

## REFERENCES

- [1] A. Lesnicar and R. Marquardt, "An innovative modular multilevel converter topology suitable for a wide power range," in *IEEE Bologna PowerTech Conf*, 2003, pp. 1–6.
- [2] S. Allebrod, R. Hamerski, and R. Marquardt, "New transformerless, scalable modular multilevel converters for HVDC-transmission," in *2008 IEEE Power Electronics Specialists Conference*, 2008, pp. 174–179.
- [3] J. Peralta, H. Saad, S. Dennerière, J. Mahseredjian, and S. Nguéfeu, "Detailed and averaged models for a 401-level MMC-HVDC system," *Transactions on Power Delivery*, vol. 27, no. 3, pp. 1501–1508, 2012.
- [4] A. S. Al-Khayyat, A. A. Ridha, and H. Fadel "Performance analysis of capacitor voltage balancing in modular multilevel converter by sorting algorithm", *International Journal of Power Electronics and Drive Systems*, vol. 13, no. 3, pp. 1548-1557, 2022.
- [5] F. Z. Peng, J. S. Lai, Jonh W. McKeever, and James VanCoevering, "A multilevel voltage-source inverter with separate DC sources for static Var generation," in *IAS '95. Conference Record of the 1995 IEEE Industry Applications Conference Thirtieth IAS Annual Meeting*, Orlando, FL, USA, 1995, pp. 2541-2548 vol.3.
- [6] R. Sharma and V. H. Makwana, "An advanced LVRT controlled DSCC-STATCOM for reactive power compensation", *International Journal of Power Electronics and Drive Systems*, vol. 14, no. 1, pp. 294-303, 2023.
- [7] M. Hagiwara, K. Nishimura, and H. Akagi, "A medium-voltage motor drive with a modular multilevel PWM inverter," *IEEE Transactions on Power Electronics*, vol. 25, no. 7, pp. 1786–1799, 2010.
- [8] A. J. Korn, M. Winkelkemper, and P. Steimer, "Low output frequency operation of the modular multi-level converter," in *2010 IEEE Energy Conversion Congress and Exposition*, 2010, pp. 3993–3997.
- [9] M. Hagiwara, I. Hasegawa, and H. Akagi, "Start-up and low-speed operation of an electric motor driven by a modular multilevel cascade inverter," *IEEE Transactions on Industry Applications*, vol. 49, no. 4, pp. 1556–1565, 2013.
- [10] A. Antonopoulos, L. Ångquist, S. Norrga, K. Ilves, L. Harnefors, and H. P. Nee, "Modular multilevel converter AC motor drives with constant torque from zero to nominal speed," *IEEE Transactions on Industry Applications*, vol. 50, no. 3, pp. 1982–1993, 2014.
- [11] S. Debnath, J. Qin, and M. Saeedifard, "Control and stability analysis of modular multilevel converter under low-frequency operation," *IEEE Transactions on Industrial Electronics*, vol. 62, no. 9, pp. 5329–5339, 2015.
- [12] M. Espinoza, R. Cárdenas, M. Díaz, and J. C. Clare, "An enhanced dq-based vector control system for modular multilevel converters feeding variable-speed drives," *IEEE Transactions on Industrial Electronics*, vol. 64, no. 4, pp. 2620–2630, 2017.
- [13] B. Li et al., "An improved circulating current injection method for modular multilevel converters in variable-speed drives," *IEEE Transactions on Industrial Electronics*, vol. 63, no. 11, pp. 7215–7225, 2016.
- [14] A. Antonopoulos, L. Ångquist, L. Harnefors, and H. P. Nee, "Optimal selection of the average capacitor voltage for variable-speed drives with modular multilevel converters," *IEEE Transactions on Power Electronics*, vol. 30, no. 1, pp. 227–234, 2015.
- [15] B. Li, Y. Zhang, G. Wang, W. Sun, D. Xu and W. Wang, "A modified modular multilevel converter with reduced capacitor voltage fluctuation," *IEEE Transactions on Industrial Electronics*, vol. 62, no. 10, pp. 6108-6119, Oct. 2015.
- [16] D. D. Le and D. -C. Lee, "A modular multilevel converter topology with novel middle submodules to reduce capacitor voltage fluctuations," *IEEE Transactions on Power Electronics*, vol. 37, no. 1, pp. 70-75, Jan. 2022.
- [17] M. Huang, J. Zou, X. Ma, Y. Li and M. Han, "Modified modular multilevel converter to reduce submodule capacitor voltage ripples without common-mode voltage injected," *IEEE Transactions on Industrial Electronics*, vol. 66, no. 3, pp. 2236-2246, March 2019.
- [18] M. Huang, Z. Kang, W. Li, J. Zou, X. Ma and J. Li, "Modified modular multilevel converter with third-order

- harmonic voltage injection to reduce submodule capacitor voltage ripples," *IEEE Transactions on Power Electronics*, vol. 36, no. 6, pp. 7074-7086, June 2021.
- [19] S. Du, B. Wu, N. R. Zargari, and Z. Cheng, "A flying-capacitor modular multilevel converter for medium-voltage motor drive," *IEEE Transactions on Power Electronics*, vol. 32, no. 3, pp. 2081–2089, 2017.
- [20] D. D. Le and D.-C. Lee, "Reduction of half-arm current stresses and flying-capacitor voltage ripples of flying-capacitor MMCs," *IEEE Access*, vol. 8, pp. 180076–180086, 2020.
- [21] S. Du, B. Wu and N. R. Zargari, "Current Stress Reduction for Flying-capacitor modular multilevel converter," *IEEE Transactions on Power Electronics*, vol. 34, no. 1, pp. 184-191, Jan. 2019.
- [22] S. Du, B. Wu, K. Tian, N. R. Zargari and Z. Cheng, "An active cross-connected modular multilevel converter (AC-MMC) for a medium-voltage motor drive," *IEEE Transactions on Industrial Electronics*, vol. 63, no. 8, pp. 4707-4717, Aug. 2016.
- [23] IGBT-Infineon Technol., "FF450R33T3E3," 2018. <https://www.infineon.com/> (accessed May. 10, 2024).
- [24] Powersim, "Tutorial IGBT and MOSFET loss calculation in the thermal module," 2019. <https://powersimtech.com/> (accessed Nov. 05, 2020).